Proposal of a directly measurable parameter quantifying the halo nature of one-neutron nuclei

Masanobu Yahiro, Shin Watanabe,* Masakazu Toyokawa, and Takuma Matsumoto
Department of Physics, Kyushu University, Fukuoka 819-0395, Japan
(Received 23 February 2016; published 20 June 2016)

We propose a measurable parameter $\mathcal{H}$ quantifying the halo nature of one-neutron halo nuclei (a) and investigate the properties of $\mathcal{H}$, assuming the core + neutron ($c+n$) model for a. The parameter $\mathcal{H}$ is defined by $\mathcal{H} = [\sigma_{\rm abs}(a) - \sigma_{\rm abs}(c)]/\sigma_{\rm abs}(n)$ with directly measurable absorption cross sections $\sigma_{\rm abs}$ of a, c, and n scattering at the same incident energy per nucleon. It varies with the one-neutron separation energy S_n in a range of $0 \leqslant \mathcal{H} \leqslant 1$, and the halo structure is most developed when $\mathcal{H} = 1$. This situation is realized only for s-wave halo nuclei in the $S_n = 0$ limit. We consider ^{11}Be and ^{15,19}C as s-wave halo nuclei, ^{31}Ne and ^{37}Mg as p-wave halo nuclei, and ^{17}C as an example of d-wave nonhalo nuclei. For each of halo nuclei, the value of $\mathcal{H}$ is deduced at a measured S_n from measured total reaction cross sections for c, n, and a scattering at intermediate and high incident energies where projectile breakup effects are negligible. The location of the resulting $(S_n,\mathcal{H})$ is plotted in the S_n-$\mathcal{H}$ plane. The empirical values of $\mathcal{H}$ at the measured S_n are extrapolated to small S_n with model calculations based on the eikonal + adiabatic approximation. In the S_n-$\mathcal{H}$ plane, the model lines are well separated into three groups of s-wave halo, p-wave halo, and d-wave nonhalo particularly in the vicinity of $S_n = 0$, and the s-wave halo lines are always above the other lines, since only the s-wave halo lines can reach a point $(S_n,\mathcal{H}) = (0,1)$ independently of the concrete form of the interaction between c and n. The relation among the three kinds of lines may be universal for any halo nucleus with small S_n. The point $(S_n,\mathcal{H}) = (0,1)$ can be regarded as a scale-invariant point in the sense that the z-integrated neutron density characterizing halo structure is invariant under the scale transformation there.

DOI: 10.1103/PhysRevC.93.064609

I. INTRODUCTION

Neutron-rich nuclei near the neutron dripline have exotic properties not seen in stable nuclei because of the weak-binding nature. In particular, some nuclei have the halo structure in which a core nucleus is surrounded by a so-called halo of orbiting extra neutron(s). For example, ^{11}Be and ^{15,19}C are s-wave one-neutron halo nuclei [1–4], while ^{6}He, ^{11}Li, ^{14}Be, and ^{22}C are Borromean nuclei with two-neutron halos [5–8]. The halo structure was first discovered by Tanihata *et al.* through a sudden enhancement in measured interaction cross sections $\sigma_{\rm I}$ for lighter isotopes [1,5]. After that, $\sigma_{\rm I}$ and total reaction cross sections $\sigma_{\rm R}$ were systematically measured to find halo nuclei [9,10]. Very recently, the measurements were done for relatively heavier nuclei like Ne and Mg isotopes [11,12], and it was reported in Refs. [11–15] that ^{31}Ne and ^{37}Mg are p-wave one-neutron halo nuclei. The sudden enhancement of measured $\sigma_{\rm R}$ is a good indicator of finding of halo nuclei experimentally, but the relation between the enhancement and the binding energy (ε) of halo nucleon is not well understood, particularly in the vicinity of $\varepsilon = 0$, as shown below.

Let us discuss the relation for one-neutron halo nuclei. The halo nuclei (a) are described by the core + nucleon ($c+n$) two-body model, and the scattering of a from a target T is well explained by the $c+n+$T three-body model. The three-body system is illustrated in Fig. 1. We assume that the projectile ($a = c+n$) has no bound excited state in order to simplify our discussion. The total reaction cross section $\sigma_{\rm R}(a)$ for a + T scattering is related to the corresponding absorption cross section $\sigma_{\rm abs}(a)$ as

$$\sigma_{\rm R}(a) = \sigma_{\rm abs}(a) + \sigma_{\rm br}(a). \tag{1}$$

In $\sigma_{\rm abs}(a)$, n and/or c are absorbed into T, and in the elastic-breakup cross section $\sigma_{\rm br}(a)$, the projectile a is broken up into c and n with no excitation of T; see, for example, Refs. [16–18] for the derivation of Eq. (1). For incident energies higher than 80 MeV/nucleon and lighter targets like ^{12}C, projectile breakup effects on $\sigma_{\rm R}$ are small. In fact, this was confirmed by the continuum-discretized coupled-channels method (CDCC) [19–21] for ^{31}Ne + ^{12}C at $E_{\rm in}/A_{\rm P} =$ 240 MeV [13] and for ^{15}C + ^{12}C scattering at $E_{\rm in}/A_{\rm P} =$ 83 MeV [22]. For the scattering, we can identify measured $\sigma_{\rm R}(a)$ with $\sigma_{\rm abs}(a)$ and can determine the matter radius $\bar{r}_a$ of a from measured $\sigma_{\rm R}(a)$ by assuming the black-sphere scattering:

$$\sigma_{\rm R}(a) \approx \sigma_{\rm abs}(a) \propto \pi[\bar{r}_a + \bar{r}_{\rm T}]^2. \tag{2}$$

Note that the matter radius $\bar{r}_{\rm T}$ of T is known. The radii $\bar{r}_a$ and $\bar{r}_{\rm T}$ are the root mean square (rms) matter radii: $\bar{r}_a = \sqrt{\langle r^2\rangle_a}$ and $\bar{r}_b = \sqrt{\langle r^2\rangle_{\rm T}}$. It is well known that $\langle r^2\rangle_a$ is divergent for s- and p-wave one-neutron halo nuclei with zero binding energy [23]. If this result is simply applied to Eq. (2), one can reach the conclusion that $\sigma_{\rm abs}(a)$ diverges. However, this conclusion is not true, as clarified below.

Glauber showed that the absorption cross section $\sigma_{\rm abs}(d)$ of deuteron (d) scattering is smaller than the sum of the absorption cross sections, $\sigma_{\rm abs}(p)$ and $\sigma_{\rm abs}(n)$, of proton (p) and neutron (n) scattering [24]: $\sigma_{\rm abs}(d) < \sigma_{\rm abs}(p) + \sigma_{\rm abs}(n)$. He considered high-energy nucleon-deuteron scattering as a concrete example. In his calculation, he took the eikonal and

*Present address: RIKEN, Nishina Center, Wako, Saitama 351-0198, Japan.

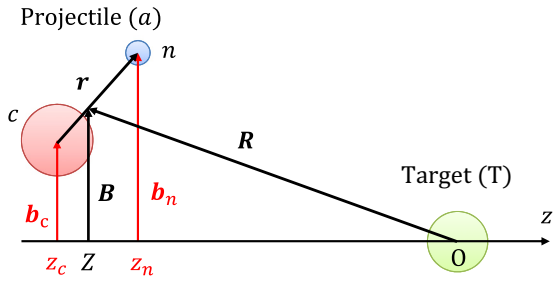

FIG. 1. Three-body system.

adiabatic approximations and assumed

$$\rho_d(\boldsymbol{r}) = \left(4\pi r_0^2\right)^{-1}\delta(|\boldsymbol{r}| - r_0), \tag{3}$$

for the deuteron density ρ_d, where $\boldsymbol{r}$ denotes the separation of two nucleons and r_0 means the range of $\rho_d(\boldsymbol{r})$. He showed that Eq. (3) is a rather good approximation for high-energy nucleon-deuteron scattering. Taking the same procedure for the scattering of one-neutron halo nucleus ($a = c + n$), one can get

$$\sigma_{\rm abs}(a) \approx \sigma_{\rm abs}(c) + \sigma_{\rm abs}(n) - \frac{\langle r^{-2}\rangle}{2\pi}\sigma_{\rm abs}(c)\sigma_{\rm abs}(n), \tag{4}$$

where $\sigma_{\rm abs}$(P) denotes an absorption cross section for a projectile P(=a,c,n), $\boldsymbol{r}$ stands for the separation between n and c, and $\langle r^{-2}\rangle$ means the expectation value of an operator r^{-2} for the ground state $\phi(\boldsymbol{r})$ of the $c + n$ system. The formula (4) shows that $\sigma_{\rm abs}(a)$ has an upper bound $\sigma_{\rm abs}(c) + \sigma_{\rm abs}(n)$; i.e., the enhancement of $\sigma_{\rm abs}(a)$ from $\sigma_{\rm abs}(c)$ has an upper bound $\sigma_{\rm abs}(n)$. This is an interesting result, but the accuracy of Eq. (4) should be checked. In particular, it should be investigated whether the assumption

$$\rho(\boldsymbol{r}) = \left(4\pi r_0^2\right)^{-1}\delta(|\boldsymbol{r}| - r_0) \tag{5}$$

for the neutron density $\rho(\boldsymbol{r})$ is valid.

In this paper, we first propose a parameter $\mathcal{H}$ quantifying the halo nature of one-neutron halo nuclei a, assuming the $c + n$ model for a. The halo parameter

$$\mathcal{H} = \frac{\sigma_{\rm abs}(a) - \sigma_{\rm abs}(c)}{\sigma_{\rm abs}(n)} \tag{6}$$

represents an enhancement of $\sigma_{\rm abs}(a)$ from $\sigma_{\rm abs}(c)$ relative to $\sigma_{\rm abs}(n)$ and is a function of one-neutron separation energy S_n. The relation between $\mathcal{H}$ and S_n is clarified both analytically and phenomenologically, particularly in the vicinity of $S_n = 0$. In the $c + n$ two-body model, the neutron binding energy ε is often identified with S_n. We take the same assumption also in this paper.

Applying the eikonal + adiabatic approximation for a + T scattering, we will show the inequality

$$\sigma_{\rm abs}(c) \leqslant \sigma_{\rm abs}(a) \leqslant \sigma_{\rm abs}(c) + \sigma_{\rm abs}(n), \tag{7}$$

and prove that the upper bound of $\sigma_{\rm abs}(a)$ is realized only for s-wave halo nuclei in the $S_n = 0$ limit, independently of the concrete form of the interaction $V(r)$ between n and c. Equation (7) shows that $\mathcal{H}$ can vary with S_n in a range of $0 \leqslant \mathcal{H} \leqslant 1$.

As a similar concept of $\mathcal{H}$, the parameter P was introduced in Ref. [23] to estimate the probability of finding a halo neutron beyond the range of the potential between c and n. The P is defined as

$$P = \frac{O}{I + O} \tag{8}$$

with

$$I = \int_0^{r_{\rm b}} R(r)r^2dr, \tag{9}$$

$$O = \int_{r_{\rm b}}^{\infty} R(r)r^2dr \tag{10}$$

for the radial wave function $R(r)$, where $r_{\rm b}$ is the border parameter between the inner and outer regions of the potential. The probability parameter P is easy to understand, but cannot be measured directly. Meanwhile, $\mathcal{H}$ corresponds to the ratio of a cross section of a extra neutron existing beyond the effective range of $\sigma_{\rm abs}(c)$ into $\sigma_{\rm abs}(n)$. The parameters P and $\mathcal{H}$ are conceptually close to each other. However, as an important advantage of $\mathcal{H}$ compared to P, the parameter $\mathcal{H}$ is directly measurable, since so are the cross sections. We can then discuss the behavior of $\mathcal{H}$ by comparison with the experimental data as shown below.

We consider ^{11}Be and ^{15,19}C as s-wave halo nuclei, ^{31}Ne and ^{37}Mg as p-wave halo nuclei, and ^{17}C as an example of d-wave nonhalo nuclei. For each a, we deduce an empirical value of $\mathcal{H}$ at the measured value of S_n from measured $\sigma_{\rm R}(a)$, $\sigma_{\rm R}(c)$, and $\sigma_{\rm R}(n)$ at intermediate and high energies, in which $\sigma_{\rm R}$ can be regarded as $\sigma_{\rm abs}$ since $\sigma_{\rm br}$ is negligibly small compared with $\sigma_{\rm R}$. The location of $(S_n,\mathcal{H})$ thus obtained is plotted in the S_n-$\mathcal{H}$ plane. The empirical values of $\mathcal{H}$ at the measured S_n are extrapolated to the vicinity of $S_n = 0$ with the $c + n$ + T model. We show that only the s-wave halo lines can reach a point $(S_n,\mathcal{H}) = (0,1)$ in the S_n-$\mathcal{H}$ plane, independently of the concrete form of $V(r)$. As a result of this property, in the S_n-$\mathcal{H}$ plane, the s-wave halo lines are always above the p-wave halo and d-wave nonhalo lines at least in $S_n < 1$ MeV. Particularly in the vicinity of $S_n = 0$, the lines are well separated into three groups of s-wave halo, p-wave halo, and d-wave nonhalo. This property may be universal for any a. We also show that the point $(S_n,\mathcal{H}) = (0,1)$ can be regarded as a scale-invariant point, since the z-integrated neutron density characterizing halo structure is invariant under the scale transformation there.

In the $S_n = 0$ limit, it is well known that $\langle r^2\rangle$ is divergent for s- and p-wave halos [23]. This result is independent of the concrete form of $V(r)$. Meanwhile, $\langle r^{-2}\rangle$ is zero only for s-wave halos in the limit, as shown later. This result is also independent of the concrete form of $V(r)$. These interesting properties are understood from the viewpoint of scale invariance.

We derive the Glauber formula (4) with an approximation more reasonable than Eq. (5), and show from the viewpoint of scale invariance that the Glauber formula is valid only for s-wave halos in the vicinity of $S_n = 0$.

In Sec. II A, Eq. (7) is derived with the eikonal and adiabatic approximations. In Sec. II B, it is proven that $\mathcal{H} = 1$ is realized only for s-wave halos with no binding energy. In

Sec. II C, we investigate properties of physical quantities in the $S_n = 0$ limit from the viewpoint of scale invariance. In Sec. III, the location of s-wave halo, p-wave halo, and d-wave nonhalo nuclei is plotted in the S_n-$\mathcal{H}$ plane. The empirical points are extrapolated to the vicinity of $S_n = 0$ with the $c + n + \mathrm{T}$ model. The validity of the Glauber formula (4) is also investigated. Section IV is devoted to a summary.

II. THEORETICAL ANALYSES

A. Absorption cross section

We consider the three-body system composed of a core nucleus (c) of mass m_c, a neutron (n) of mass m_n, and a target nucleus (T) of mass m_T. The three-body system is illustrated in Fig. 1; here, $\boldsymbol{R} = (\boldsymbol{B}, Z)$ stands for the coordinate of a projectile ($a = c + n$) from T, while $\boldsymbol{r} = (\boldsymbol{b}, z)$ corresponds to the coordinate of n from c.

Using the eikonal + adiabatic approximation [25], one can describe the absorption cross section $\sigma_\mathrm{abs}(a)$ for a + T scattering as [26–28]

$$\sigma_\mathrm{abs}(a) = \int d\boldsymbol{B}\left[1 - \int d\boldsymbol{r}|\mathcal{S}_c\mathcal{S}_n|^2\rho(r)\right] \tag{11}$$

with the S matrices of $c + A$ and $n + A$ scattering

$$\mathcal{S}_c(b_c) = \exp\left[\frac{1}{i\hbar v}\int_{-\infty}^{\infty} dz_c U_c(r_c)\right], \tag{12}$$

$$\mathcal{S}_n(b_n) = \exp\left[\frac{1}{i\hbar v}\int_{-\infty}^{\infty} dz_n U_n(r_n)\right], \tag{13}$$

and the neutron density

$$\rho(r) = \frac{1}{2\ell+1}\sum_m \left|\frac{u_\ell(r)}{r}Y_{\ell m}(\hat{r})\right|^2 = \frac{1}{4\pi}\left|\frac{u_\ell(r)}{r}\right|^2, \tag{14}$$

where $\phi_{\ell m}(\boldsymbol{r}) = u_\ell(r)Y_{\ell m}(\hat{r})/r$ is the normalized ground-state wave function of the $c + n$ subsystem with the angular momentum ℓ and its z component m, and $\boldsymbol{r}_c = \boldsymbol{R} - m_n\boldsymbol{r}/m_a$ and $\boldsymbol{r}_n = \boldsymbol{R} + m_c\boldsymbol{r}/m_a$ for $m_a = m_c + m_n$. Here, $U_x(r_x)$ is the optical potential between $x(=c,n)$ and T, and $\boldsymbol{r}_x = (\boldsymbol{b}_x, z_x)$ is the coordinate between x and T. The velocity v is related to the incident energy E_in in the laboratory system as $E_\mathrm{in} = m_a v^2/2$, since the present model is formulated under nonrelativistic kinematics. For x + T scattering with the same v as a + T scattering, the reaction and absorption cross sections, $\sigma_\mathrm{R}(x)$ and $\sigma_\mathrm{abs}(x)$, are obtained by

$$\sigma_\mathrm{R}(x) = \sigma_\mathrm{abs}(x) = \int d\boldsymbol{b}_x[1 - |\mathcal{S}_x(b_x)|^2]. \tag{15}$$

Note that the incident energies per nucleon are common among a, n, and c scattering.

Using the identity

$$1 - |\mathcal{S}_c|^2|\mathcal{S}_n|^2 = (1 - |\mathcal{S}_c|^2) + (1 - |\mathcal{S}_n|^2) - (1 - |\mathcal{S}_c|^2)(1 - |\mathcal{S}_n|^2), \tag{16}$$

one can easily show from Eqs. (11) and (15) that

$$\sigma_\mathrm{abs}(a) = \sigma_\mathrm{abs}(c) + \sigma_\mathrm{abs}(n) - \Delta \tag{17}$$

for

$$\Delta = \int d\boldsymbol{b}_n(1 - |\mathcal{S}_n(b_n)|^2)\int d\boldsymbol{b}\bar{\rho}(b)(1 - |\mathcal{S}_c(b_c)|^2) \tag{18}$$

with the z-integrated neutron density

$$\bar{\rho}(b) = \int_{-\infty}^{\infty} dz\rho(r) = \frac{1}{4\pi}\int_{-\infty}^{\infty} dz\left|\frac{u_\ell(r)}{r}\right|^2. \tag{19}$$

The optical potential $U_x(r_x)$ has a finite range ν_x, and hence the b integration in Eq. (18) has an upper bound $b_\mathrm{max} \sim \nu_c + \nu_n$. Thus, Δ is determined by $\bar{\rho}(b)$ in *a finite range* $0 \leqslant b \leqslant b_\mathrm{max}$. Inserting Eq. (17) into (6) leads to

$$\mathcal{H} = \frac{\sigma_\mathrm{abs}(n) - \Delta}{\sigma_\mathrm{abs}(n)}. \tag{20}$$

This indicates that $\mathcal{H}$ is sensitive to $\bar{\rho}(b)$. E_in dependence of $\mathcal{H}$ is almost canceled between the numerator and the denominator, so that $\mathcal{H}$ little depends on E_in, as shown in Sec. III C.

Because of $\Delta \geqslant 0$, we have the inequality

$$\sigma_\mathrm{abs}(a) \leqslant \sigma_\mathrm{abs}(c) + \sigma_\mathrm{abs}(n). \tag{21}$$

The equality is realized only for s-wave halos in the zero-binding limit, as shown in Sec. II B.

Because of $0 \leqslant |\mathcal{S}_n|^2 \leqslant 1$, we have the inequality

$$1 - |\mathcal{S}_c|^2 \leqslant 1 - |\mathcal{S}_c|^2|\mathcal{S}_n|^2. \tag{22}$$

Using Eq. (22) in Eq. (11) and making the variable transformation from $\boldsymbol{B}$ to $\boldsymbol{b}_c$, one can obtain the lower bound of $\sigma_\mathrm{abs}(c)$,

$$\sigma_\mathrm{abs}(c) \leqslant \sigma_\mathrm{abs}(a), \tag{23}$$

where c is assumed to be inert. The equality $\sigma_\mathrm{abs}(a) = \sigma_\mathrm{abs}(c)$ is realized for example for a proton target in lower-incident energy, since U_n is a nucleon-nucleon potential with no imaginary part. If $\sigma_\mathrm{abs}(a) < \sigma_\mathrm{abs}(c)$, it means that c is shrunk by an extra neutron (n). Such an effect is seen for isotopes ^{16}C and ^{32}Ne next to halo nuclei ^{15}C and ^{31}Ne [22,29]. However, this effect is considered to be small for halo nuclei themselves, since n is far from c. Combining Eq. (23) with Eq. (21) leads to Eq. (7).

Particularly at $b = 0$, $\bar{\rho}(b)$ is related to the expectation value $\langle r^{-2}\rangle$ for the ground state as

$$\bar{\rho}(0) = \int_{-\infty}^{\infty} dz\rho(z) = \frac{1}{2\pi}\int_0^{\infty} dr\left|\frac{u_\ell(r)}{r}\right|^2 = \frac{1}{2\pi}\int d\boldsymbol{r}\left|\frac{u_\ell(r)}{r}Y_{\ell m}(\hat{r})\right|^2\frac{1}{r^2} = \frac{1}{2\pi}\langle r^{-2}\rangle. \tag{24}$$

If $\bar{\rho}(b)$ has no b dependence in a range of $0 \leqslant b \leqslant b_\mathrm{max}$, Δ becomes

$$\Delta \approx \frac{1}{2\pi}\langle r^{-2}\rangle\sigma_\mathrm{abs}(c)\sigma_\mathrm{abs}(n). \tag{25}$$

Thus we can obtain Eq. (4) without the approximation (5). However, the b dependence of $\bar{\rho}(b)$ is not negligible in a range of $0 \leqslant b \leqslant b_\mathrm{max}$, as shown later in Sec. III. An exception is s-wave halos in the zero-binding limit. In this case, $\bar{\rho}(b)$ vanishes for any value of b; see Sec. II B for the proof. Equation (4) is

thus useful for s-wave halos in the vicinity of the weak-binding limit.

B. Halo state in the weak-binding limit

For later convenience, we consider the unnormalized ground-state wave function $\tilde{u}_\ell(r)$ of the $c+n$ system. It is governed by the Schrödinger equation

$$\left(-\frac{\hbar^2}{2\mu}\frac{d^2}{dr^2}+\frac{\hbar^2}{2\mu}\frac{\ell(\ell+1)}{r^2}+V(r)\right)\tilde{u}_\ell(r)=-\varepsilon\tilde{u}_\ell(r) \quad (26)$$

with the reduced mass $\mu=m_n m_c/(m_n+m_c)$ and a nuclear potential $V(r)$. Here we assume that $V(r)$ has a finite range $r_{\rm v}$ and then $V(r)=0$ at $r\geqslant r_m$ for a value r_m somewhat larger than $r_{\rm v}$.

We start with the case of $\ell=0$. The magnitude of $\tilde{u}_0(r)$ is set to 1 at $r=r_m$, and $\tilde{u}_0(r)$ is divided into the internal wave function $\tilde{u}_0^{\rm int}(r)$ in a range of $0\leqslant r<r_m$ and the external one

$$\tilde{u}_0^{\rm ext}(r)=\frac{\exp(-\kappa r)}{\exp(-\kappa r_m)} \quad (27)$$

in a range of $r\geqslant r_m$. The norm F_0 of $\tilde{u}_0(r)$ is obtained by

$$F_0=\int_0^\infty dr|\tilde{u}_0(r)|^2=F_0^{\rm int}+F_0^{\rm ext} \quad (28)$$

with

$$F_0^{\rm int}=\int_0^{r_m}dr\left|\tilde{u}_0^{\rm int}(r)\right|^2, \quad (29)$$

$$F_0^{\rm ext}=\int_{r_m}^\infty dr\left|\tilde{u}_0^{\rm ext}(r)\right|^2=\frac{1}{2\kappa}. \quad (30)$$

Obviously, $F_0^{\rm int}$ is finite for any κ, but $F_0^{\rm ext}$ diverges at $\kappa=0$.

Using $\tilde{u}_0(r)$ and F_0, one can get

$$\bar{\rho}(b)=\frac{1}{4\pi F_0}\int_{-\infty}^\infty dz\left|\frac{\tilde{u}_0(r)}{r}\right|^2. \quad (31)$$

In Eq. (31), the z integration is finite even in the limit of $\kappa=0$, because of the factor $1/r^2$. Hence, $\bar{\rho}(b)$ is zero in the $\kappa=0$ limit for any b, since $F_0^{\rm ext}$ diverges in the limit. Therefore, $\langle r^{-2}\rangle$ and Δ become zero in the limit; note that $\bar{\rho}(b)$ contributes to Δ only in a finite range of $0\leqslant b\leqslant b_{\rm max}$. This result does not depend on the concrete form of $V(r)$, as far as it is short ranged. The equality in Eq. (21) is thus realized for s-wave halos with zero binding energy. This is true not only for a lowest-energy state but also for excited states, if the binding energy is zero. In fact, for the case of ^{11}Be, the $0s$ state is a forbidden state, and the $1s$ state is the ground state with a small binding energy. The equality in Eq. (21) is realized also for the case of a deformed core nucleus, if the last neutron is dominated by the s-wave component in the weak binding limit [30].

Next we consider the case of $\ell\geqslant 1$. Again, we consider the unnormalized wave function $\tilde{u}_\ell(r)$ that is 1 at $r=r_m$. The wave function can be divided into the internal part $\tilde{u}_\ell^{\rm int}(r)$ at $0\leqslant r<r_m$ and the external part

$$\tilde{u}_\ell^{\rm ext}(r)=\frac{i\kappa r h_\ell^{(1)}(i\kappa r)}{i\kappa r_m h_\ell^{(1)}(i\kappa r_m)} \quad (32)$$

at $r\geqslant r_m$, where $h_\ell^{(1)}(x)$ is the spherical Hankel function of the first kind. The norm F_ℓ of $\tilde{u}_\ell(r)$ is given by

$$F_\ell=\int_0^\infty dr|\tilde{u}_\ell(r)|^2=F_\ell^{\rm int}+F_\ell^{\rm ext} \quad (33)$$

with

$$F_\ell^{\rm int}=\int_0^{r_m}dr\left|\tilde{u}_\ell^{\rm int}(r)\right|^2 \quad (34)$$

and

$$F_\ell^{\rm ext}=\int_{r_m}^\infty dr\left|\tilde{u}_\ell^{\rm ext}(r)\right|^2\to\frac{r_m}{2\ell-1} \quad (35)$$

for $\kappa r_m\ll 1$, because of

$$\tilde{u}_\ell^{\rm ext}(r)\to\left(\frac{r_m}{r}\right)^\ell \quad (\kappa r\ll 1). \quad (36)$$

The z-integrated neutron density is described by

$$\bar{\rho}(b)=\frac{1}{4\pi F_\ell}\int_{-\infty}^\infty dz\left|\frac{\tilde{u}_\ell(r)}{r}\right|^2. \quad (37)$$

In the $\kappa=0$ limit, F_ℓ is finite in Eq. (37), so that $\bar{\rho}(b)$, $\langle r^{-2}\rangle$, and Δ become finite.

C. Scale invariance

As shown in Sec. II B, $\bar{\rho}(b)$, $\langle r^{-2}\rangle$, and Δ are zero for s-wave halos with zero binding energy. This result does not depend on the concrete form of $V(r)$. Similarly, it is well known that $\langle r^2\rangle$ is divergent for s- and p-wave halos with zero binding energy, independently of the concrete form of $V(r)$ [23]. In this subsection, we consider these properties from the viewpoint of scale invariance, since it is shown as an important result of the nuclear effective field theory that scale invariance is an essential concept in the limit of $\varepsilon=0$ [31].

We then perform the scale transformation $\boldsymbol{r}\to\lambda\boldsymbol{r}$ in the Schrödinger equation (26) and multiply the resulting equation by a factor λ^2:

$$\left(-\frac{\hbar^2}{2\mu}\frac{d^2}{dr^2}+\frac{\hbar^2}{2\mu}\frac{\ell(\ell+1)}{r^2}+\lambda^2V(\lambda r)\right)\tilde{u}_\ell(\lambda r)$$
$$=-\frac{\hbar^2(\lambda\kappa)^2}{2\mu}\tilde{u}_\ell(\lambda r), \quad (38)$$

where λ is a positive number. Equation (38) shows that $\tilde{u}_\ell(\lambda r)$ is an eigenstate generated by a potential $\lambda^2V(\lambda r)$ and the binding energy is $\varepsilon=(\hbar\lambda\kappa)^2/(2\mu)$. We now consider the following scale transformation

$$\tilde{u}_\ell(r)\to\tilde{u}_\ell(\lambda r),\quad V(r)\to\lambda^2V(\lambda r),\quad \kappa\to\lambda\kappa \quad (39)$$

instead of the original one $\boldsymbol{r}\to\lambda\boldsymbol{r}$, where note that $\boldsymbol{r}$ is not scaled in the new scale transformation (39). Particularly in the $\kappa=0$ limit of our interest, $\tilde{u}_\ell(\lambda r)$ is an eigenstate with $\varepsilon=0$ for any λ. In other words, once $V(r)$ generates an eigenstate with $\varepsilon=0$, the scaled potential $\lambda^2V(\lambda r)$ can do so for any λ. Thus, there are an infinite number of potentials generating eigenstates with $\varepsilon=0$.

The range of $\lambda^2V(\lambda r)$ is r_v/λ. Hence one should divide $\tilde{u}_\ell(\lambda r)$ into the internal part $\tilde{u}_\ell^{\rm int}(\lambda r)$ at $r<r_m/\lambda$ and the

external one $\tilde{u}_\ell^{\rm ext}(\lambda r)$ at $r \geqslant r_m/\lambda$. The Schrödinger equation for the external part is

$$\left(-\frac{\hbar^2}{2\mu}\frac{d^2}{dr^2}+\frac{\hbar^2}{2\mu}\frac{\ell(\ell+1)}{r^2}\right)\tilde{u}_\ell^{\rm ext}(\lambda r)=0 \tag{40}$$

in the zero-binding limit. The kinetic operator does not include any λ. This means that we can derive a λ-independent external wave function $\mathcal{I}_\ell^{\rm ext}(r)$ by multiplying $\tilde{u}_\ell^{\rm ext}(\lambda r)$ by a λ-dependent factor. This will be done below. If the expectation value of an operator is determined only from $\mathcal{I}_\ell^{\rm ext}(r)$ and thereby independent of $\lambda^2 V(\lambda r)$, the value is obviously scale invariant. Therefore, if the expectation value of some operator does not depend on the concrete form of $V(r)$, the expectation value is scale invariant.

The scaled wave function $\tilde{u}_\ell(\lambda r)$ is 1 at $r = r_m/\lambda$, because

$$\tilde{u}_\ell^{\rm ext}(\lambda r)=\frac{i\kappa\lambda r h_\ell^{(1)}(i\kappa\lambda r)}{i\kappa r_m h_\ell^{(1)}(i\kappa r_m)} \tag{41}$$

at $r \geqslant r_m/\lambda$. The external wave function $\tilde{u}_\ell^{\rm ext}(\lambda r)$ tends to $[r_m/(\lambda r)]^\ell$ in the $\kappa = 0$ limit. If we consider $\mathcal{I}_\ell(r) = \lambda^\ell \tilde{u}_\ell(\lambda r)$ in the limit, the external part $\mathcal{I}_\ell^{\rm ext}(r) = \lambda^\ell \tilde{u}_\ell^{\rm ext}(\lambda r) = (r_m/r)^\ell$ becomes independent of λ (scale invariant), although the internal part $\mathcal{I}_\ell^{\rm int}(r) = \lambda^\ell \tilde{u}_\ell^{\rm int}(\lambda r)$ does not. Thus, the fact that physical quantities are independent of the concrete form of $V(r)$ in the $\kappa = 0$ limit means that the quantities are scale invariant in the limit.

Let us consider a dimensionful operator r^n for n being -2 or a positive integer, and calculate the expectation value $\langle r^n\rangle_\lambda$ with the ground-state wave function $\lambda^\ell \tilde{u}_\ell(\lambda r)Y_{\ell m}(\hat{r})/r$. For finite κ, the value is finite and has the relation

$$\langle r^n\rangle_\lambda=\frac{\int_0^\infty dr\lambda^{2\ell}|\tilde{u}_\ell(\lambda r)|^2 r^n}{\int_0^\infty dr\lambda^{2\ell}|\tilde{u}_\ell(\lambda r)|^2}=\lambda^{-n}\langle r^n\rangle, \tag{42}$$

where $\langle r^n\rangle$ denotes the expectation value at $\lambda = 1$. The relation (42) is true also in the $\kappa = 0$ limit. Thus, the expectation value of dimensionful operator becomes scale variant, when the value is finite. In other words, scale invariance is realized only when the value is either zero or infinity. Therefore, when the expectation value of dimensionful operator is scale invariant in the $\kappa = 0$ limit and hence becomes independent of the concrete form of $V(r)$, the value becomes either zero or infinity.

Now we explicitly evaluate the scaled expectation values $\langle r^{-2}\rangle_\lambda$ and $\langle r^2\rangle_\lambda$ and the scaled neutron density $\bar{\rho}_\lambda(b)$. Since the overall factor λ^ℓ of the wave function $\lambda^\ell \tilde{u}_\ell(\lambda r)Y_{\ell m}(\hat{r})/r$ does not affect the values, we consider $\tilde{u}_\ell(\lambda r)Y_{\ell m}(\hat{r})/r$ for simplicity.

Making the same discussion as in Sec. II B, one can obtain the norm $F_0(\lambda) = F_0^{\rm int}(\lambda) + F_0^{\rm ext}(\lambda)$ with

$$F_0^{\rm int}(\lambda)=\int_0^{r_m/\lambda} dr\left|\tilde{u}_0^{\rm int}(\lambda r)\right|^2=\frac{F_0^{\rm int}(1)}{\lambda}, \tag{43}$$

$$F_0^{\rm ext}(\lambda)=\int_{r_m/\lambda}^{\infty} dr\left|\tilde{u}_0^{\rm ext}(\lambda r)\right|^2=\frac{1}{2\kappa r_m}\frac{r_m}{\lambda} \tag{44}$$

for $\ell = 0$. As for $\ell \geqslant 1$, we have the norm $F_\ell(\lambda) = F_\ell^{\rm int}(\lambda) + F_\ell^{\rm ext}(\lambda)$ with

$$F_\ell^{\rm int}(\lambda)=\int_0^{r_m/\lambda} dr\left|\tilde{u}_\ell^{\rm int}(\lambda r)\right|^2=\frac{F_\ell^{\rm int}(1)}{\lambda}, \tag{45}$$

$$F_\ell^{\rm ext}(\lambda)=\int_{r_m/\lambda}^{\infty} dr\left|\tilde{u}_\ell^{\rm ext}(\lambda r)\right|^2\to\frac{r_m}{\lambda(2\ell-1)} \tag{46}$$

for $\kappa r_m \ll 1$.

For s-wave halos in the limit of $\kappa = 0$, $F_0^{\rm ext}$ diverges independently of λ, so that

$$\bar{\rho}_\lambda(b)=\frac{1}{4\pi F_0(\lambda)}\int_{-\infty}^{\infty} dz\left|\frac{\tilde{u}_0(\lambda r)}{r}\right|^2=0 \tag{47}$$

for any finite λ and b, where we note that the $\kappa = 0$ limit is taken after the z integration. Equation (47) is true also for infinite b, as shown in the Appendix. Consequently, $\bar{\rho}(b)$ and $\langle r^{-2}\rangle = 2\pi\bar{\rho}(0)$ are scale invariant in the $\kappa = 0$ limit. For $\ell \geqslant 1$, meanwhile, $\bar{\rho}(b)$ are finite and scale variant in the $\kappa = 0$ limit, since so is F_ℓ.

As for $\langle r^2\rangle_\lambda$, direct calculations for $\ell = 0$ show that

$$\begin{aligned}\langle r^2\rangle_\lambda &\to \frac{1}{F_0(\lambda)}\left[\int_0^{r_m/\lambda} dr r^2\left|\tilde{u}_0^{\rm int}(\lambda r)\right|^2+\frac{1}{4}\frac{1}{(\kappa r_m)^3}\frac{r_m^3}{\lambda^3}\right]\\ &\to \frac{1}{2}\frac{1}{(\kappa r_m)^2}\frac{r_m^2}{\lambda^2}\end{aligned} \tag{48}$$

for $\kappa r_m \ll 1$. As for $\ell = 1$, we get

$$\langle r^2\rangle_\lambda \to \frac{1}{F_1(\lambda)}\left[\int_0^{r_m/\lambda} dr r^2\left|\tilde{u}_1^{\rm int}(\lambda r)\right|^2+\frac{5}{4}\frac{1}{\kappa r_m}\frac{r_m^3}{\lambda^3}\right] \tag{49}$$

for $\kappa r_m \ll 1$. For s- and p-wave halos in the limit of $\kappa = 0$, $\langle r^2\rangle_\lambda$ are thus divergent for any λ, and hence $\langle r^2\rangle$ becomes scale invariant in the $\kappa = 0$ limit. Note that the $\kappa = 0$ limit is taken after integration.

III. PHENOMENOLOGICAL ANALYSES

A. Derivation of halo parameter

For later convenience, we define the mass numbers of projectile (P) and T as $A_{\rm P}$ and $A_{\rm T}$, respectively. The halo parameter $\mathcal{H}$ is obtainable from measured $\sigma_{\rm R}(c)$, $\sigma_{\rm R}(n)$, and $\sigma_{\rm R}(a)$ for lighter targets like ^{12}C and $E_{\rm in}/A_{\rm P} > 80$ MeV where projectile-breakup effects are small on $\sigma_{\rm R}$ [13,22], since the measured $\sigma_{\rm R}$ can be regarded as $\sigma_{\rm abs}$ there with good accuracy.

We consider ^{11}Be and ^{15,19}C as s-wave halo nuclei and ^{31}Ne and ^{37}Mg as p-wave halo nuclei. For comparison, ^{17}C is also considered as an example of nonhalo nuclei with small ε; in the simple shell-model picture with no residual interaction, the last neutron is in a $0d$ orbital. We take ^{12}C as a target nucleus, since experimental data on $\sigma_{\rm R}$ are richest for this target. As for $\sigma_{\rm R}(c)$ and $\sigma_{\rm R}(c+n)$, the experimental data are available at $E_{\rm in}/A_{\rm P} = 790$ MeV for ^{10,11}Be, at $E_{\rm in}/A_{\rm P} \sim 960$ MeV for $^{16-19}$C, and at $E_{\rm in}/A_{\rm P} = 240$ MeV for ^{30,31}Ne [11] and ^{36,37}Mg [12]; for the systems ^{30,31}Ne, $\sigma_{\rm I}$ were measured, but $\sigma_{\rm I}$ were confirmed to be very close to $\sigma_{\rm R}$ [14].

For ^{14}C + ^{12}C scattering, the experimental data are available on $\sigma_{\rm R}$ at $E_{\rm in}/A_{\rm P} = 83$ MeV and $\sigma_{\rm I}$ at $E_{\rm in}/A_{\rm P} = 965$ MeV, whereas, for ^{15}C + ^{12}C scattering, the data are available on

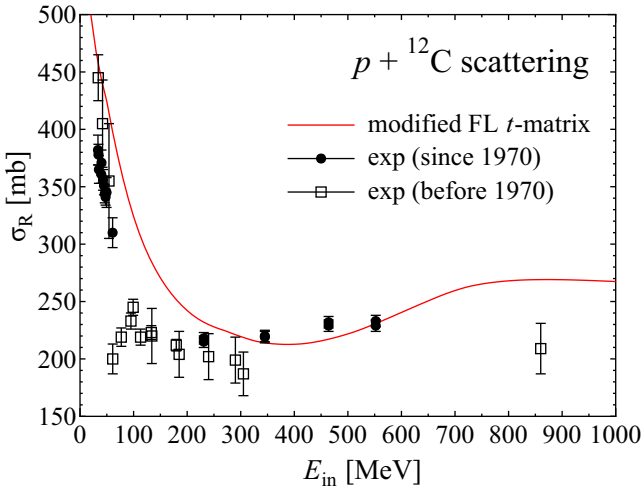

FIG. 2. Total reaction cross sections for $p + {}^{12}$C scattering as a function of E_{in}.

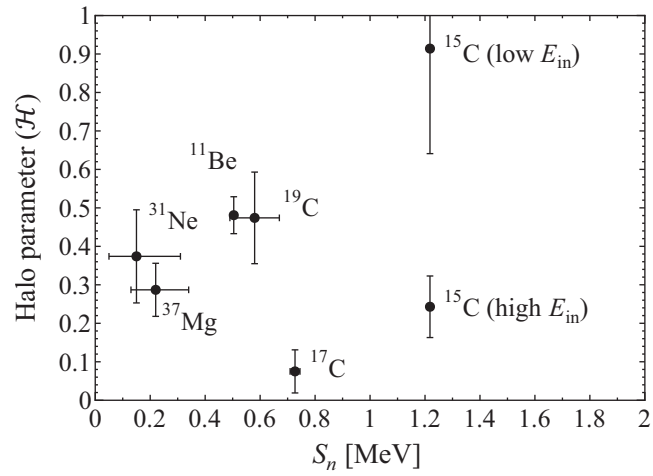

FIG. 3. Location of halo nuclei in the parameter S_n-$\mathcal{H}$ plane. Experimental or empirical data on S_n are taken from Refs. [35–37]. See the text for the derivation of $\mathcal{H}$.

σ_R at $E_{in}/A_P = 83$ and σ_I at $E_{in}/A_P \sim 740$ MeV. It is confirmed with the Glauber model that σ_R little depends on E_{in}/A_P in a range of $700 \lesssim E_{in}/A_P \lesssim 1000$ MeV for ^{12}C + ^{12}C scattering [32]. We then assume that σ_I at 740 MeV is identical with σ_I at 965 MeV, and deduce empirical values of $\mathcal{H}$ for $E_{in}/A_P = 83$ and 965 MeV.

In general, $\sigma_R(n)$ is not available at the same E_{in}/A_P as $\sigma_R(c)$ and $\sigma_R(c+n)$. We then use the single-folding (SF) model to evaluate the $\sigma_R(n)$. In the SF model, U_n is obtained by folding an effective nucleon-nucleon (NN) interaction with the phenomenological ^{12}C density [33] determined from electron scattering. In the present formulation of Sec. II A for nucleon-nucleus and nucleus-nucleus scattering, nonrelativistic kinematics is assumed. Hence, the effective NN interaction, i.e., the NN t matrix, should be determined from NN data with nonrelativistic kinematics. In this case, all relativistic effects on NN scattering are implicitly included in the t matrix itself. This t matrix can be easily obtained by modifying the Franey-Love (FL) t matrix [34] slightly to reproduce NN data. This t matrix is referred to as the modified FL t matrix in this paper.

The SF model is now applied to $p + {}^{12}$C scattering, and the total reaction cross section $\sigma_R(p)$ is calculated with Eq. (15). Figure 2 shows E_{in} dependence of $\sigma_R(p)$. The solid line denotes the model result, while the closed circles and open squares stand for experimental data since and before 1970, respectively. In the lower-energy region $E_{in} < 150$ MeV, the SF model overestimates the experimental data sizably. This may come from the fact that nuclear-medium effects are not included in the present t-matrix SF model. Meanwhile in the higher-energy region $E_{in} \gtrsim 230$ MeV of our interest, the newer data have smaller error bars than the older ones, and the newer data tend to be larger than the older ones. We then respect the newer data. The SF model well reproduces the newer data in $E_{in} = 231$–552 MeV, although it overestimates the older data at $E_{in} = 860$ MeV slightly. This good agreement with the newer data may indicate that the present t-matrix SF model is reliable in the higher-energy region. The total reaction cross section $\sigma_R(n)$ for $n + {}^{12}$C scattering is then calculated with the t-matrix SF model without introducing any adjustable parameter.

An exception is the derivation of $\sigma_R(n)$ at $E_{in} = 83$ MeV. The t-matrix SF model for $p + {}^{12}$C scattering overestimates the newer data at $E_{in} = 33$–61 MeV. We then multiply the folding potential U_p by the normalization factor f_N to reproduce the data. The resulting factor $f_N = 0.6$ is used for U_n, since the model calculation shows that the difference between $\sigma_R(n)$ and $\sigma_R(p)$ is small. Eventually, the value of f_N is 0.6 for $E_{in} = 83$ MeV and 1 for $E_{in} \geqslant 240$ MeV.

Figure 3 shows the location of discovered one-neutron halo nuclei in the S_n-$\mathcal{H}$ plane. For comparison, ^{17}C is also plotted as an example of nonhalo nuclei with small S_n. Two results are presented for ^{15}C; one is determined from $\sigma_R(n)$, $\sigma_R(c)$, and $\sigma_R(c+n)$ at $E_{in}/A_P = 83$ MeV and the other is from those at $E_{in}/A_P = 960$ MeV. The two results are consistent with each other within the 2σ deviation, but non-negligible difference between the mean values of the two results shows that the value of $\mathcal{H}$ is ambiguous for ^{15}C. For the other nuclei, the resulting $\mathcal{H}$ have error bars small enough to make qualitative discussions. For this reason, we mainly consider the nuclei except ^{15}C. The E_{in} dependence of $\mathcal{H}$ for ^{15}C will be discussed in Sec. III C. As seen in Fig. 3, p-wave halo nuclei ^{31}Ne and ^{37}Mg have smaller $\mathcal{H}$ than s-wave halo nuclei ^{11}Be and ^{19}C, and $\mathcal{H}$ is even smaller for a d-wave nonhalo nucleus ^{17}C.

B. Halo parameter in the vicinity of the weak-binding limit

No halo nucleus is discovered at extremely small S_n such as $S_n \ll 0.01$ MeV. We then do the following $c + n +$ T model calculation to see the behavior of $\mathcal{H}$ in the vicinity of $S_n = 0$. The ground state $u_\ell(r)$ of the $c + n$ system is described with the Woods-Saxon potential determined by the well-depth method; namely, the depth parameter V_0 is tuned to measured S_n with the radius and diffuseness parameters fixed at the standard values $1.27A_c^{1/3}$ fm and 0.67 fm [38], where A_c is the mass number of c. The potential U_c between c and T is obtained by folding the modified FL t matrix with the densities

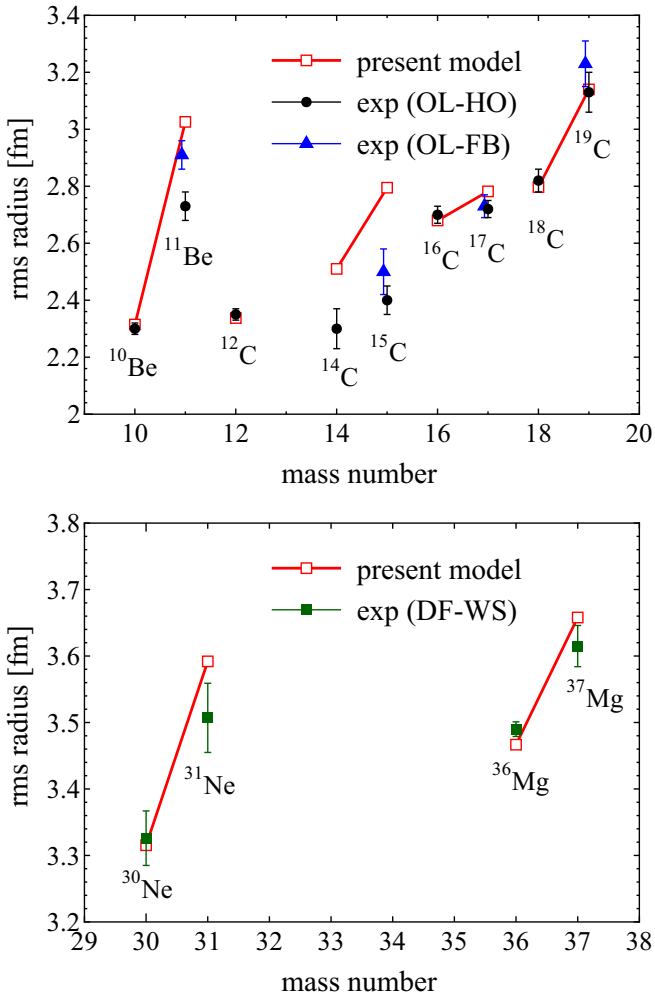

FIG. 4. Root mean square (rms) matter radii of core and halo nuclei. The open squares stand for the results of the present model, while the closed circles, closed triangles, and closed squares denote the experimental data deduced from $\sigma_{\rm R}$ and $\sigma_{\rm I}$ with the optical-limit Glauber model based on harmonic-oscillator projectile densities (OL-HO), the optical-limit Glauber model based on few-body model densities (OL-FB) [9,10], and the double-folding model based on Woods-Saxon model densities (DF-WS) [15]. For ^{12}C, the closed circle represents the phenomenological density [33] determined from electron scattering.

of c and T. In the double-folding model, the density of c is calculated with the spherical Hartree-Fock (HF) method with the Gogny-D1S interaction [39] for ^{10}Be and ^{14,16,18}C and with antisymmetrized molecular dynamics (AMD) with the Gogny-D1S interaction for ^{30}Ne and ^{36}Mg. In the AMD calculations, deformation effects are taken into account [13,15]. The folding potential U_c is normalized to reproduce the corresponding data on $\sigma_{\rm R}(c)$. The normalization factors f_c are 0.69 for ^{10}Be, 0.54, 0.71, and 0.70 for ^{14,16,18}C, 0.65 for ^{30}Ne, and 0.66 for ^{36}Mg.

In order to confirm the accuracy of the present model, we calculate rms matter radii $\bar{r}_c$ and $\bar{r}_a$ of c and a. The results are shown in Fig. 4 for ^{10,11}Be, ^{14,15}C, ^{16,17}C, ^{18,19}C, ^{30,31}Ne, and ^{36,37}Mg. The model results (open squares) are consistent with the experimental data deduced from measured $\sigma_{\rm R}$ and $\sigma_{\rm I}$ with

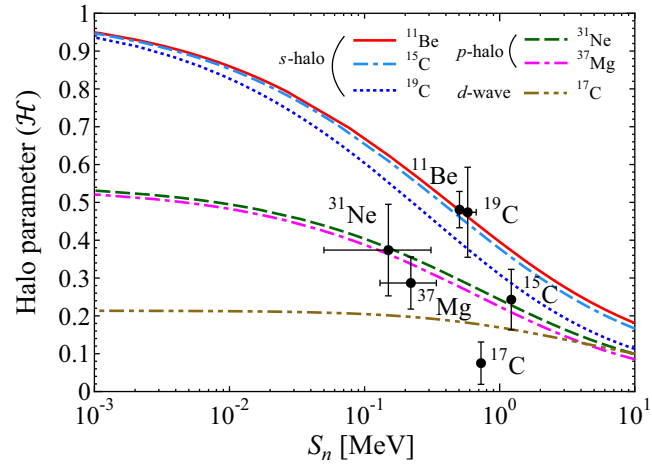

FIG. 5. Behavior of $\mathcal{H}$ in the vicinity of $S_n = 0$. A logarithmic scale is taken for the horizontal axis. The theoretical results are shown by a solid (dotted) line for ^{11}Be (^{19}C), by a dashed (long and short dashed) line for ^{31}Ne (^{37}Mg), by a long and two short dashed line for ^{17}C and by a short and two long dashed line for ^{15}C. See Fig. 3 for the experimental data.

the optical-limit Glauber model based on harmonic-oscillator-type projectile densities (closed circles), the optical-limit Glauber model based on few-body model densities (closed triangles) [9,10], and the double-folding model based on Woods-Saxon model densities (closed squares) [15]. Precisely, the present model overestimates the experimental data slightly for ^{14,15}C. However, the deviation does not affect $\mathcal{H}$, because U_c is normalized to reproduce the measured $\sigma_{\rm R}(c)$. For a while, we do not consider the case of $E_{\rm in}/A_{\rm P} = 83$ MeV for ^{14,15}C, since the data on $\bar{r}_a$ and $\bar{r}_c$ are deduced from $\sigma_{\rm R}(c)$ and $\sigma_{\rm R}(a)$ at $E_{\rm in}/A_{\rm P} = 960$ MeV.

Figure 5 shows the behavior of $\mathcal{H}$ in the vicinity of $S_n = 0$. Here a logarithmic scale is taken for the S_n axis, and only the case of $E_{\rm in}/A_{\rm P} = 960$ MeV is considered for ^{15}C. As for halo nuclei ^{11}Be, ^{19}C, ^{31}Ne, and ^{37}Mg, the results of the present model are consistent with the corresponding experimental data within the 1σ deviation. As for ^{15,17}C, the model results are consistent with the corresponding data within the 2σ deviation. As expected, the theoretical lines reach the scale-invariant point $(S_n, \mathcal{H}) = (0,1)$ only for s-wave halo nuclei ^{11}Be, ^{15}C, and ^{19}C. The values of $\mathcal{H}$ in the $S_n = 0$ limit are about 0.55 for p-wave halo nuclei ^{31}Ne and ^{37}Mg and about 0.21 for a d-wave non-halo nucleus ^{17}C. In the vicinity of $S_n = 0$, consequently, the six lines are well separated into three groups of s-wave halo, p-wave halo, and d-wave nonhalo. This separation may be universal for any unstable nucleus with small S_n. Therefore, if $\sigma_{\rm R}(p)$, $\sigma_{\rm R}(c)$, and $\sigma_{\rm R}(a)$ are newly measured at the same $E_{\rm in}/A_{\rm P}$ for unstable nuclei with small S_n and $\mathcal{H}$ are calculated, one can see the halo nature of the nuclei through the values of $\mathcal{H}$ without making any model calculation.

Figure 6 shows the behavior of the probability parameter P defined by Eq. (8) in the vicinity of $S_n = 0$. Since we cannot determine the border parameter $r_{\rm b}$ uniquely for the ambiguity coming from the diffuseness parameter in the Woods-Saxon potential, we take $r_{\rm b} = \sqrt{\frac{5}{3}\langle r^2\rangle_{\rm WS}}$ as a plausible example,

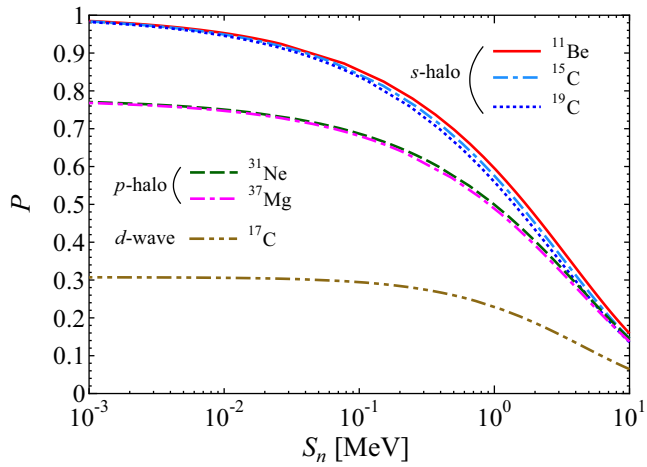

FIG. 6. Same as Fig. 5 but for the probability parameter P defined by Eq. (8).

where $\langle r^2\rangle_{\rm WS}$ is the mean square radius of the Woods-Saxon potential. Note that the mean square radius of square-well potential with the radius $r_{\rm b}$ becomes equal to $\langle r^2\rangle_{\rm WS}$ in the above condition. The probability parameter P is almost similar to $\mathcal{H}$ qualitatively. The parameter $\mathcal{H}$ is thus a useful way of understanding P qualitatively and a measurable parameter quantifying the halo nature.

C. $E_{\rm in}$ dependence of halo parameter for ^{15}C+^{12}C scattering

Here we discuss $E_{\rm in}$ dependence of $\mathcal{H}$ in Fig. 7 for ^{15}C+^{12}C scattering. As for $\mathcal{H}$, two empirical values were deduced from

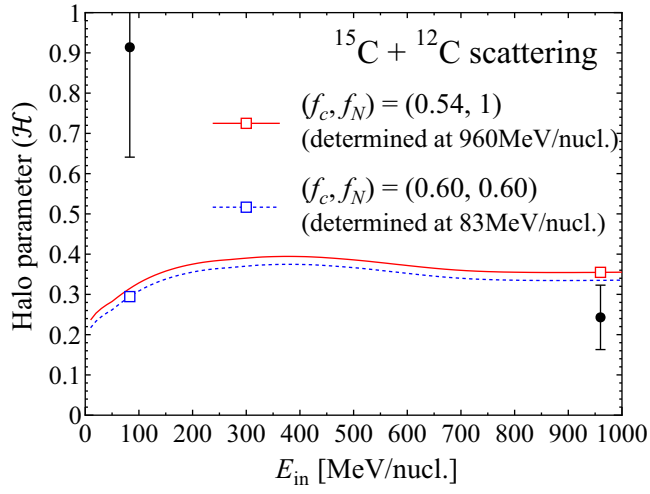

FIG. 7. Halo parameter $\mathcal{H}$ as a function of $E_{\rm in}/A_{\rm P}$ for ^{15}C+^{12}C scattering. The empirical value of $\mathcal{H}$ is taken from Fig. 3. The model results are shown by open squares at $E_{\rm in}/A_{\rm P}=83$ and 960 MeV. Here, the normalization factors are $(f_c,f_N)=(0.54,1)$ for $E_{\rm in}/A_{\rm P}=960$ MeV and $(f_c,f_N)=(0.60,0.60)$ for $E_{\rm in}/A_{\rm P}=83$ MeV. The model results are extrapolated to other $E_{\rm in}$ by assuming that the normalization factors f_c and f_N do not depend on $E_{\rm in}$. The solid (dashed) line stands for the model result of $(f_c,f_N)=(0.54,1)$ $[(f_c,f_N)=(0.60,0.60)]$.

experimental data on $\sigma_{\rm R}(c)$ and $\sigma_{\rm R}(a)$ at $E_{\rm in}/A_{\rm P}=83$ and 960 MeV, as shown in Fig. 3. We first compare the empirical values with the model results at the two incident energies. For this purpose, the normalization factors f_c and f_N are determined from experimental data on $\sigma_{\rm R}(c)$ and $\sigma_{\rm R}(p)$ at the incident energies. The resulting values are $f_c=0.54$ and $f_N=1$ for $E_{\rm in}/A_{\rm P}=960$ MeV and $f_c=0.6$ and $f_N=0.6$ for $E_{\rm in}/A_{\rm P}=83$ MeV. The $\mathcal{H}$ calculated with these normalization factors are plotted by open squares at the two energies. The model calculations overestimate the empirical value at $E_{\rm in}/A_{\rm P}=960$ MeV but underestimate at $E_{\rm in}/A_{\rm P}=83$ MeV. Next, the two model results (open squares) are extrapolated to other $E_{\rm in}$ with f_c and f_N fixed at either $(f_c,f_N)=(0.54,1)$ or $(f_c,f_N)=(0.6,0.6)$. The solid and dashed lines denote the model results of $(f_c,f_N)=(0.54,1)$ and $(f_c,f_N)=(0.6,0.6)$, respectively. The two lines are close to each other and have weak $E_{\rm in}$ dependence. This may indicate that $\mathcal{H}$ is nearly independent of $E_{\rm in}$. As an interesting result, the model prediction lies halfway between two empirical values for $\mathcal{H}$. It is then highly expected that measurements of $\sigma_{\rm R}$ will be made for ^{14,15}C at typical beam energies of the Radioactive Isotope Beam Factory at RIKEN ($E_{\rm in}/A_{\rm P}\sim 250$ MeV).

D. Validity of the Glauber formula

Finally we investigate the validity of the Glauber formula (4). As shown in Sec. II A, this formula is valid when $\bar\rho(b)$ is independent of b in a range of $0\leqslant b\leqslant b_{\rm max}\approx 15$ fm. This condition is automatically satisfied, when $\bar\rho(b)$ is scale invariant, i.e., $\bar\rho(b)=\bar\rho(\lambda b)$ for any λ. The Glauber formula is thus related to scale invariance of $\bar\rho(b)$.

Inserting Eq. (4) into Eq. (6) leads to

$$\mathcal{H}\approx\mathcal{H}_{\rm Gl}\equiv 1-\frac{1}{2\pi}\langle r^{-2}\rangle\sigma_{\rm abs}(c). \tag{50}$$

As shown in Fig. 8, $\bar\rho(b)$ has large b dependence in $0\leqslant b\leqslant b_{\rm max}\approx 15$ fm for all cases of the s-wave halo nucleus

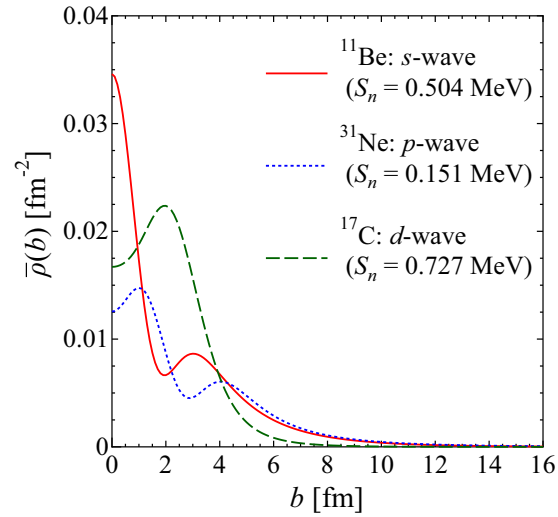

FIG. 8. b dependence of z-integrated projectile densities ^{11}Be, ^{17}C, and ^{31}Ne. The solid, dashed, and dotted lines denote the b dependence for ^{11}Be, ^{17}C, and ^{31}Ne, respectively.

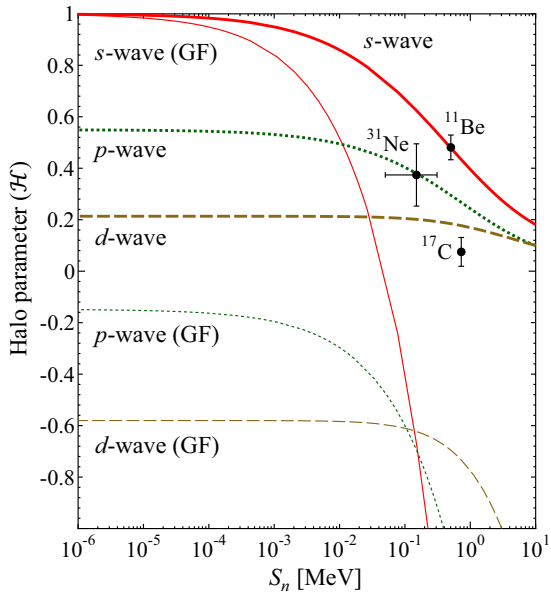

FIG. 9. Test of the Glauber formula for in the S_n-$\mathcal{H}$ plane. Exact results (thick lines) are compared with approximate results (thin lines) based on the Glauber formula (GF) of Eq. (4). The solid, dashed, and dotted lines indicate the cases of ^{11}Be, ^{17}C, and ^{31}Ne, respectively.

^{11}Be, the p-wave halo nucleus ^{31}Ne, and the d-wave nonhalo nucleus ^{17}C. In Fig. 9, the Glauber formula is directly tested in the S_n-$\mathcal{H}$ plane. The $\mathcal{H}$ values calculated exactly without the Glauber formula are plotted by thick lines, and the $\mathcal{H}_{\rm Gl}$ values calculated approximately with the Glauber formula are drawn by thin lines; here the solid, dashed, and dotted lines correspond to the model results for ^{11}Be, ^{17}C, and ^{31}Ne, respectively. The $\mathcal{H}_{\rm Gl}$ are largely deviated from the corresponding $\mathcal{H}$ except for the case of s-wave halo in the vicinity of $S_n = 0$. This result is natural, since $\bar{\rho}(b)$ is scale invariant only at the point $(S_n,\mathcal{H}) = (0,1)$.

IV. SUMMARY

We proposed a measureable parameter $\mathcal{H}$ quantifying the halo nature of one-neutron halo nuclei a, assuming the $c+n$ model for a. We proved the inequality (7). This equation shows that the halo parameter $\mathcal{H}$ of Eq. (6) can vary with S_n in a range of $0 \leqslant \mathcal{H} \leqslant 1$. Since the halo structure is most developed when $\mathcal{H} = 1$, we proved that this situation is realized only for s-wave halos in the $S_n = 0$ limit, independently of the concrete form of the interaction $V(r)$ between c and n.

We considered ^{11}Be and ^{15,19}C as s-wave halo nuclei, ^{31}Ne and ^{37}Mg as p-wave halo nuclei, and ^{17}C as an example of d-wave nonhalo nuclei. For each halo nucleus, an empirical value of $\mathcal{H}$ was deduced at the measured S_n from experimental data on $\sigma_{\rm R}(a)$, $\sigma_{\rm R}(c)$, and $\sigma_{\rm R}(n)$ at intermediate and high incident energies where $\sigma_{\rm br}$ is negligibly small compared with $\sigma_{\rm R}$, and $\sigma_{\rm R}$ can be regarded as $\sigma_{\rm abs}$. The parameter $\mathcal{H}$ is thus a measurable parameter. This point is an important advantage compared to the probability parameter P that is almost similar to $\mathcal{H}$ qualitatively but cannot be measured directly. The location of $(S_n,\mathcal{H})$ thus obtained is plotted in the S_n-$\mathcal{H}$ plane. The empirical points are extrapolated to the vicinity of $S_n = 0$ by using the $c+n$ + T model. As mentioned above, only the s-wave halo lines can reach a point $(S_n,\mathcal{H}) = (0,1)$ in the S_n-$\mathcal{H}$ plane, independently of the concrete form of $V(r)$. As a result of this property, the s-wave halo lines are always above the p-wave halo and d-wave nonhalo lines at least in $S_n < 1$ MeV in the S_n-$\mathcal{H}$ plane. Particularly in the vicinity of $S_n = 0$, the lines are well separated into three groups of s-wave halo, p-wave halo, and d-wave nonhalo. This separation may be universal for any unstable nuclei with small S_n. Therefore, if $\sigma_{\rm R}(a)$, $\sigma_{\rm R}(c)$, and $\sigma_{\rm R}(n)$ are newly measured at the same $E_{\rm in}/A_{\rm P}$ for unstable nuclei with small S_n and empirical values of $\mathcal{H}$ are deduced from the experimental data, one can see the halo nature of the nuclei through the values without making any model calculation.

In the $S_n = 0$ limit, $\bar{\rho}(b)$ and $\langle r^{-2}\rangle$ are zero for s-wave halo nuclei, whereas $\langle r^2\rangle$ is divergent for s- and p-wave halo nuclei. These results are independent of the concrete form of $V(r)$, indicating that the quantities are determined only from the external part of the ground-state wave function $\tilde{u}_\ell(r)$ of the $c+n$ system. Since $\tilde{u}_\ell(r)$ can be defined so that the external part becomes scale invariant in the $S_n = 0$ limit, $\bar{\rho}(b)$ and $\langle r^{-2}\rangle$ for s-wave halos and $\langle r^2\rangle$ for s- and p-wave halos turn out to be scale invariant in the limit. Any dimensionful quantity is scale invariant only when it is either zero or infinity. This is the reason why the dimensionful scale-invariant quantities, $\bar{\rho}(b)$, $\langle r^{-2}\rangle$, and $\langle r^2\rangle$, become either zero or infinity in the $S_n = 0$ limit. The point $(S_n,\mathcal{H}) = (0,1)$ in the S_n-$\mathcal{H}$ can be regarded as a scale-invariant point in the sense that $\bar{\rho}(b)$ is scale invariant there.

Finally we tested the validity of the Glauber formula (4). This formula is valid, when $\bar{\rho}(b)$ is independent of b in $0 \leqslant b \leqslant b_{\rm max} \approx 15$ fm. This condition is automatically satisfied, when $\bar{\rho}(b)$ is scale invariant. The Glauber formula is thus good only for s-wave halos in the vicinity of $S_n = 0$, i.e., near the scale-invariant point.

ACKNOWLEDGMENTS

The authors are grateful to M. Fukuda and M. Takechi for valuable discussions. One of the authors, S.W., appreciates R. F. Casten and organizers of the TALENT school (Course 5: Theory for exploring nuclear structure experiments) held in GANIL, Caen, France, in August 2014, which triggered some of the analyses in this paper. This work was supported by JSPS KAKENHI Grants No. 26400278 and No. 25·4319.

APPENDIX: SCALE INVARIANCE OF $\bar{\rho}_\lambda(b)$

In this Appendix, we re-examine the scale-transformed z-integrated density of Eq. (47)

$$\bar{\rho}_\lambda(b) = \frac{1}{4\pi F_0(\lambda)} \int_{-\infty}^{\infty} dz \left| \frac{\tilde{u}_0(\lambda r)}{r} \right|^2 \qquad \text{(A1)}$$

and show that the scale invariance of $\bar{\rho}_\lambda(b)$ is realized not only for finite b but also for infinite b.

Let us consider finite b_1 and b_2 satisfying the condition $r_m < b_1 < b_2$. Obviously, the inequality

$$0 \leqslant \bar{\rho}_\lambda(b_2) \leqslant \bar{\rho}_\lambda(b_1) \tag{A2}$$

is satisfied because of the relation

$$0 \leqslant \frac{\left|\tilde{u}_0\left(\lambda\sqrt{b_2^2+z^2}\right)\right|^2}{b_2^2+z^2} \leqslant \frac{\left|\tilde{u}_0\left(\lambda\sqrt{b_1^2+z^2}\right)\right|^2}{b_1^2+z^2} \tag{A3}$$

for the integrand in Eq. (A1). On the other hand, we have already probed that $\bar{\rho}(b_1)$ is scale invariant for finite b_1:

$$\lim_{\kappa\to 0}\bar{\rho}(b_1) = 0. \tag{A4}$$

Using Eqs. (A2) and (A4), we can get

$$\lim_{\kappa\to 0}\bar{\rho}_\lambda(b_2) = 0 \tag{A5}$$

for infinite b_2.

[1] I. Tanihata, J. Phys. G **22**, 157 (1996).
[2] M. Fukuda *et al.*, Phys. Lett. B **268**, 339 (1991).
[3] I. Tanihata, T. Kobayashi, O. Yamakawa, S. Shimoura, K. Ekuni, K. Skugimoto, N. Takahashi, T. Shimoda, and H. Sato, Phys. Lett. B **206**, 592 (1988).
[4] T. Nakamura, N. Fukuda, N. Aoi, N. Imai, M. Ishihara, H. Iwasaki, T. Kobayashi, T. Kubo, A. Mengoni, T. Motobayashi, M. Notani, H. Otsu, H. Sakurai, S. Shimoura, T. Teranishi, Y. X. Watanabe, and K. Yoneda, Phys. Rev. C **79**, 035805 (2009).
[5] I. Tanihata, H. Hamagaki, O. Hashimoto, Y. Shida, N. Yoshikawa, K. Sugimoto, O. Yamakawa, T. Kobayashi, and N. Takahashi, Phys. Rev. Lett. **55**, 2676 (1985).
[6] T. Suzuki *et al.*, Nucl. Phys. A **658**, 313 (1999).
[7] T. Moriguchi *et al.*, Nucl. Phys. A **929**, 83 (2014).
[8] K. Tanaka, T. Yamaguchi, T. Suzuki, T. Ohtsubo, M. Fukuda, D. Nishimura, M. Takechi, K. Ogata, A. Ozawa, T. Izumikawa, T. Aiba, N. Aoi, H. Baba, Y. Hashizume, K. Inafuku, N. Iwasa, K. Kobayashi, M. Komuro, Y. Kondo, T. Kubo, M. Kurokawa, T. Matsuyama, S. Michimasa, T. Motobayashi, T. Nakabayashi, S. Nakajima, T. Nakamura, H. Sakurai, R. Shinoda, M. Shinohara, H. Suzuki, E. Takeshita, S. Takeuchi, Y. Togano, K. Yamada, T. Yasuno, and M. Yoshitake, Phys. Rev. Lett. **104**, 062701 (2010).
[9] A. Ozawa *et al.*, Nucl. Phys. A **691**, 599 (2001), and references therein.
[10] A. Ozawa, T. Suzuki, and I. Tanihata, Nucl. Phys. A **693**, 32 (2001), and references therein.
[11] M. Takechi *et al.*, Phys. Lett. B **707**, 357 (2010).
[12] M. Takechi, S. Suzuki, D. Nishimura, M. Fukuda, T. Ohtsubo, M. Nagashima, T. Suzuki, T. Yamaguchi *et al.*, Phys. Rev. C **90**, 061305 (2014).
[13] K. Minomo, T. Sumi, M. Kimura, K. Ogata, Y. R. Shimizu, and M. Yahiro, Phys. Rev. Lett. **108**, 052503 (2012).
[14] T. Sumi, K. Minomo, S. Tagami, M. Kimura, T. Matsumoto, K. Ogata, Y. R. Shimizu, and M. Yahiro, Phys. Rev. C **85**, 064613 (2012).
[15] S. Watanabe, K. Minomo, M. Shimada, S. Tagami, M. Kimura, M. Takechi, M. Fukuda, D. Nishimura *et al.*, Phys. Rev. C **89**, 044610 (2014).
[16] K. Yabana, Y. Ogawa, and Y. Suzuki, Nucl. Phys. A **539**, 295 (1992).
[17] M. Yahiro, K. Ogata, and K. Minomo, Prog. Theor. Phys. **126**, 167 (2011).
[18] S. Hashimoto, M. Yahiro, K. Ogata, K. Minomo, and S. Chiba, Phys. Rev. C **83**, 054617 (2011).
[19] M. Kamimura, M. Yahiro, Y. Iseri, Y. Sakuragi, H. Kameyama, and M. Kawai, Prog. Theor. Phys. Suppl. **89**, 1 (1986).
[20] N. Austern, Y. Iseri, M. Kamimura, M. Kawai, G. Rawitscher, and M. Yahiro, Phys. Rep. **154**, 125 (1987).
[21] M. Yahiro, K. Ogata, T. Matsumoto, and K. Minomo, Prog. Theor. Exp. Phys. (2012) 01A206.
[22] T. Matsumoto and M. Yahiro, Phys. Rev. C **90**, 041602 (2014).
[23] K. Riisager, A. S. Jensen, and P. Møller, Nucl. Phys. A **548**, 393 (1992).
[24] R. J. Glauber, Phys. Rev. **100**, 242 (1955).
[25] R. J. Glauber, in *Lectures in Theoretical Physics* (Interscience, New York, 1959), Vol. 1, p. 315.
[26] M. S. Hussein and K. W. McVoy, Nucl. Phys. A **445**, 124 (1985).
[27] C. A. Bertulani and K. W. McVoy, Phys. Rev. C **46**, 2638 (1992).
[28] K. Hencken, G. Bertsch, and H. Esbensen, Phys. Rev. C **54**, 3043 (1996).
[29] K. Hagino and H. Sagawa, Phys. Rev. C **84**, 011303 (2011); **85**, 014303 (2012); **85**, 037604 (2012).
[30] I. Hamamoto, Phys. Rev. C **69**, 041306(R) (2004).
[31] S. Weinberg *et al.*, Nucl. Phys. B **363**, 3 (1991).
[32] W. Horiuchi, Y. Suzuki, B. Abu-Ibrahim, and A. Kohama, Phys. Rev. C **75**, 044607 (2007).
[33] H. de Vries, C. W. de Jager, and C. de Vries, At. Data Nucl. Data Tables **36**, 495 (1987).
[34] W. G. Love and M. A. Franey, Phys. Rev. C **24**, 1073 (1981); M. A. Franey and W. G. Love, *ibid.* **31**, 488 (1985).
[35] G. Audi *et al.*, Nucl. Phys. A **729**, 337 (2003).
[36] T. Nakamura, N. Kobayashi, Y. Kondo, Y. Satou, J. A. Tostevin, Y. Utsuno, N. Aoi, H. Baba, N. Fukuda, J. Gibelin, N. Inabe, M. Ishihara, D. Kameda, T. Kubo, T. Motobayashi, T. Ohnishi, N. A. Orr, H. Otsu, T. Otsuka, H. Sakurai, T. Sumikama, H. Takeda, E. Takeshita, M. Takechi, S. Takeuchi, Y. Togano, and K. Yoneda, Phys. Rev. Lett. **112**, 142501 (2014).
[37] N. Kobayashi, T. Nakamura, Y. Kondo, J. A. Tostevin, Y. Utsuno, N. Aoi, H. Baba, R. Barthelemy, M. A. Famiano, N. Fukuda, N. Inabe, M. Ishihara, R. Kanungo, S. Kim, T. Kubo, G. S. Lee, H. S. Lee, M. Matsushita, T. Motobayashi, T. Ohnishi, N. A. Orr, H. Otsu, T. Otsuka, T. Sako, H. Sakurai, Y. Satou, T. Sumikama, H. Takeda, S. Takeuchi, R. Tanaka, Y. Togano, and K. Yoneda, Phys. Rev. Lett. **112**, 242501 (2014).
[38] A. Bohr and B. R. Mottelson, *Nuclear Structure* (Benjamin, New York, 1975), Vol. I.
[39] J. F. Berger, M. Girod, and D. Gogny, Comput. Phys. Commun. **63**, 365 (1991).